

Check for updates



www.chemistryselect.org

New Naphthoquinone-Based Manganese (II) Complexes: Synthesis, Characterization, and Cytotoxicity

R. L. Machado, [a] W. T. G. Novato, [b] R. S. Silva,*[c] F. C. Demidoff, [a] S. H. M. Abe, [d] M. V. Palmeira-Mello,*[d] J. H. A. Neto, [e] J. A. Ellena, [f] A. A. Batista, [d] C. D. Netto, [a] and M. S. Schultz*[c]

We have synthesized and characterized two new complexes of stilbenes-quinone hybrids with a manganese(II) center, Mn1 [Mn(NQ1)₂(EtOH)₂] and Mn2 ([Mn(NQ2)₂(EtOH)₂], where NQ1 and NQ2 are the 2-hydroxy-3-styryl-1,4-naphthoquinone and 2-hydroxy-3-(4-chlorostyryl)-1,4-naphthoquinone in their deprotonated forms. FTIR and UV-vis spectroscopy analyses were used to verify changes in characteristic bands upon the coordination to a manganese center. Single-crystal X-ray diffraction analysis allowed the structural elucidation of Mn1 as *cis*-[Mn(NQ1)₂(EtOH)₂] and Mn2 as *cis*-[Mn(NQ2)₂(EtOH)₂] isomers. The charge distribution, dipole moments, and Gibbs free energy

of the complexes were also calculated. The in vitro cytotoxicity results revealed that the coordination of quinone nucleus into a metal center improved their cytotoxicity, highlighting the effect of the manganese complexes on ovarian cancer cells. Mn1, the promising candidate, was able to change the morphology and inhibit the colony formation in A2780 cells. Further, based on circular dichroism and fluorescence results, this manganese complex interacts with DNA via minor groove binding. In light of these results, Mn1 displays a promising skeleton for the development of more cytotoxic and selective manganese-based compounds against ovarian cancer.

1. Introduction

Naphthoquinones constitute an important group of quinones widely distributed in nature, especially in families of higher

- [a] R. L. Machado, F. C. Demidoff, C. D. Netto Instituto Multidisciplinar de Química, Universidade Federal do Rio de Janeiro, Macaé, Rio de Janeiro 27930-560, Brazil
- [b] W. T. G. Novato NQTCM - Núcleo de Química Teórica e Computacional de Macaé, Instituto Multidisciplinar de Química, Universidade Federal do Rio de Janeiro, Macaé, Rio de Janeiro 27930-560, Brazil
- [c] R. S. Silva, M. S. Schultz Instituto de Biodiversidade e Sustentabilidade, Universidade Federal do Rio de Janeiro, Macaé, Rio de Janeiro 27965-045, Brazil E-mail: s.silvaroberto1@gmail.com mss060@gmail.com
- [d] S. H. M. Abe, M. V. Palmeira-Mello, A. A. Batista Departamento de Química, Universidade Federal de São Carlos, São Carlos, São Paulo 13565-905, Brazil E-mail: marcos.palmeira@ufscar.br
- [e] J. H. A. Neto Departamento de Química Fundamental, Universidade de São Paulo, São Paulo, SP 05508-900, Brazil
- [f] J. A. Ellena Instituto de Física de São Carlos, Universidade de São Paulo, São Paulo, SP 13566-590, Brazil
- Supporting information for this article is available on the WWW under https://doi.org/10.1002/slct.202504426
- © 2025 The Author(s). ChemistrySelect published by Wiley-VCH GmbH. This is an open access article under the terms of the Creative Commons Attribution License, which permits use, distribution and reproduction in any medium, provided the original work is properly cited.

plants.^[1] These structures can be considered cyclic derivatives of naphthalene with two carbonyl groups at 1,2 or 1,4 positions (Figure 1), resulting in different chemical and physicochemical characteristics.^[2,3] 1,4-Naphthoquinones are the most stable and widespread naphthoquinones, and among them, 2-hydroxy-1,4-naphthoquinones stand out as highly researched natural substances with various applications in medicinal chemistry.^[4-7] These compounds have a wide spectrum of biological activities, such as antitumor,^[2,7] antifungal,^[8] antimicrobial,^[9,10] and antiparasitic,^[11,12] which are often attributed to their redox properties.^[4-6]

Lawsone (2-hydroxy-1,4-naphthoquinone), juglone (5hydroxy-1,4-naphthalenedione), plumbagin (5-hydroxy-2methyl-1,4- naphthoquinone) and lapachol (2-hydroxy-3-(3methyl-2-butenyl)-1,4-naphthoquinone) are the most well-known hydroxy-1,4-naphthoquinones.[2] Lawsone, the bioactive constituent of henna dye (Lawsonia inermis), has been extensively studied in organic and medicinal chemistry due to its pharmacological potential.[13] In particular, lawsone and its derivatives have been promising cytotoxic agents against several types of cancer.[14-18] Similarly, lapachol, a natural naphthoquinone isolated from the lapacho tree (Handroanthus avellanedae), is recognized for its important anticancer activity. Recognized as a key lead compound in drug design, lapachol exhibits diverse biological activities, including antiproliferative and pro-apoptotic properties, making it a valuable candidate for the development of new drugs.[19-22] Chemical modification of naturally occurring structures is an alternative in the search for new drugs, [23] atovaquone and buparvaquone are examples of synthetic hydroxynaphthoguinones clinically used as antiparasitic agents. Atovaquone, for instance, is widely used in the treatment and

43, Downloaded from thtps://chemistry-crope.onlinelibary.wiley.com/doi/10.1002/slct.20204426 by University Of Sao Paulo - Brazil, Wiley Online Library on [25/1/12025]. See the Terms and Conditions (https://onlinelibary.wikey.com/ems-and-conditions) on Wiley Online Library for rules of use; OA arcides are governed by the apaplicable Creative Commons License

Figure 1. Structures of naphthoquinone derivatives.

prophylaxis of malaria, while buparvaquone plays a crucial role in combating bovine theileriosis.^[24–26]

In addition to their pharmacological potential, 2-hydroxy-1,4-naphthoquinones are also considered good ligands for preparing coordination compounds, since the α -hydroxyketone moiety is an efficient chelator to hard cationic sites. $^{[27,28]}$ Moreover, complexation with transition metals often enhances their pharmacological profile regarding activity and selectivity, also play crucial role on the modulation of ADME (absorption, distribution, metabolism, and excretion) properties. This strategy was recently employed in designing and preparing promising metallodrugs with focus on medicinal chemistry. $^{[29-31]}$

Molecular hybridization is an important approach in medicinal chemistry used to obtain different molecules with increased cytotoxicity properties. [32-34] Based on the pharmacological potential of natural and synthetic 2-hydroxy-1,4-naphthoquinones, our research group used this technique to design a series of synthetic derivatives called stilbene-quinones (Figure 1). [35,36] These compounds incorporate the hydroxynaphthoquinone moiety from lapachol, conjugated to an arylethene group that is characteristic of another class of bioactive natural products: the naphthoquinones. [37,38] This combination resulted in a series of molecules with interesting chemical and pharmacological properties, which have also been explored in the preparation of transition-metal complexes with improved anticancer activity. [39-42]

In this context, manganese(II) compounds have emerged as an alternative to other metallodrugs.^[41] As a coenzyme, manganese plays an essential role in various biological processes such as gluconeogenesis, ammonia metabolism, and protection from oxidative stress.^[42] Furthermore, manganese is critical for antitumor immune responses and has been shown to improve the efficacy of clinical immunotherapy.^[43,44] Considering our ongoing interest in developing new coordination compounds with 2-hydroxy-1,4-naphthoquinone ligands, here we report for the first time the synthesis and characterization of two Mn(II)

complexes containing stilbene-quinone ligands (Mn1 and Mn2). The in vitro cytotoxicity of these compounds was investigated on different cell lines. To obtain biological insights regarding its action, Mn1 was further studied on A2780 ovarian cancer cells. Morphological, clonogenic, and ROS generation assays were also performed. Furthermore, DNA-binding properties were investigated by circular dichroism and fluorescence spectroscopies. Overall, our results demonstrated that Mn1 is a promising cytotoxic compound against ovarian cancer.

2. Results and Discussion

2.1. Synthesis and Characterization

Manganese complexes Mn1 and Mn2 with the general formula [Mn(NQ)₂(EtOH)₂] were prepared in ethanol medium from MnCl₂•4H₂O by replacing two chloride ligands with the corresponding stilbene-quinone ligand (HNQ1 or HNQ2), ^[35] which had been previously deprotonated by triethylamine (Scheme 1). ^[45] Both complexes were obtained as air-stable crystalline solids, soluble in DMF, DMSO, and DCM, and insoluble in ethanol, hexane, and H₂O. The molar conductance measurements in DMF at room temperature for Mn1 (26.7 Ω^{-1} cm² mol⁻¹) and Mn2 (31.6 Ω^{-1} cm² mol⁻¹) corroborate the non-electrolytic nature of the Mn(II) complexes, ^[46] suggesting the coordination of two anionic stilbene-quinone ligands to the Mn(II) ion. Moreover, the percentages of carbon and hydrogen obtained by elemental analysis agree with the theoretical values, confirming their purity.

The FTIR spectra of the free ligands present sharp $\nu(OH)$ stretch bands at 3312 (**HNQ1**) and 3260 cm⁻¹ (**HNQ2**), characteristic of the intramolecular hydrogen bond of the hydroxyl group with the neighboring carbonyl group. These bands disappear upon complexation, suggesting the complexation of the stilbene-quinones as anionic ligands and the region becomes

43, Downloaded from https://chemistry-cuope.onlinelibrary.wiley.com/doi/10.1002/slct.202504426 by University Of Sao Paulo - Brazil, Wiley Online Library on [25/11/2025]. See the Terms and Conditions (https://onlinelibrary.wiley.com/ems-and-conditions) on Wiley Online Library for rules of use; OA archies are governed by the apaplicable Creative Commons License

Scheme 1. Complexation strategy to produce Mn1 and Mn2.

defined by $\nu(OH)$ stretches of coordinated ethanol molecules, now producing broad bands at 3257 (Mn1) and 3203 cm⁻¹ (Mn2). The ν (C1=O1) absorptions in 1647 cm⁻¹ (HNQ1) and 1645 cm⁻¹ (HNQ2), shifted to 1533 cm⁻¹ and 1532 cm⁻¹, indicating the O,Obidentate coordination of the stilbene-quinones to the Mn(II) ion (chelate mode). [27,45] Finally, the ν (Mn-O) stretches appear in 487 cm⁻¹ for Mn1 and 500 cm⁻¹ for Mn2.^[45] These results agree with the theoretical IR spectra calculated for HNQ1, HNQ2, Mn1, and Mn2 (Figures S6 and S8). The electronic spectra of complexes Mn1 and Mn2 (Figures S9 and S10) present typical bands of intraligand $\pi \to \pi^*$ transitions around 335 and 380 nm for the stilbene-quinones. Moreover, an intense and broad band was observed around 570 nm, which was attributed to both intraligand $n \to \pi^*$ transitions and the metal to ligand charge transfer (MLCT) process, which are characteristic of metal complexes containing quinones as ligands. [48,49] The electrochemical behavior of complexes Mn1 and Mn2 was evaluated by cyclic voltammetry in CH₂Cl₂ (Figure 2), revealing two irreversible processes for both complexes. These processes are associated with sequential single-electron and assigned to the Mn^{II}/Mn^{III} and Mn^{III}/Mn^{IV} processes, ranging from 0 to 1000 mV and from 1000 to 1500 mV, respectively. [50-53] Since the cyclic voltammograms of the naphthoquinone-based ligands presented redox processes in the range 0-1500 mV, [54,55] it was possible to distinguish them from their complexes, supporting the attribution of the manganese(II) redox processes (Figure S11).

The molecular structures of both complexes were obtained by single-crystal X-ray crystallography (Figure 3). Complex Mn1 crystallizes in the monoclinic system, space group I2/a, while Mn1 crystallizes in the triclinic system, space group P-1 (Table 1). Both complexes display a distorted octahedral geometry around the

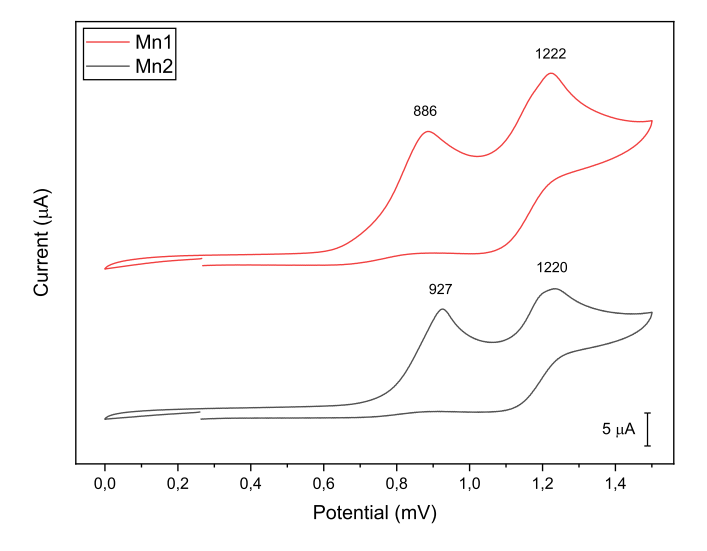


Figure 2. Cyclic voltammograms of complexes Mn1 and Mn2 measured in CH_2Cl_2 solutions containing 0.1 mol L^{-1} of $TBACIO_4$. The scans were performed in the negative direction, starting from the open circuit potential. Electrodes: reference, Ag/AgCl; working, platinum; auxiliary, platinum (scan rate = 100 mV·s⁻¹).

manganese(II) ion that can be attributed to constraints imposed by the bite angle of the stilbene-quinone ligands (\angle 01-Mn-O2 angles of 73.76° for HNQ1 and 73.55° for HNQ2). The two remaining coordination sites are occupied by ethanol molecules in a *cis* configuration, with \angle 03-Mn-O4 angles of 93.44° (Mn1) and 97.8° (Mn2) (Table S2). Complexes **Mn1** and **Mn2** show optical isomerism, and both Δ and Λ enantiomers were observed in the unit cells (Figure S12).

43, Downloaded from thtps://chemistry-crope.onlinelibary.wiley.com/doi/10.1002/slct.20204426 by University Of Sao Paulo - Brazil, Wiley Online Library on [25/1/12025]. See the Terms and Conditions (https://onlinelibary.wikey.com/ems-and-conditions) on Wiley Online Library for rules of use; OA arcides are governed by the apaplicable Creative Commons License

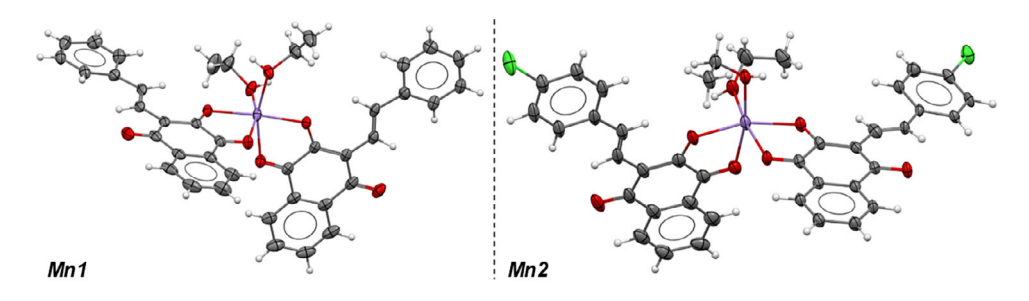


Figure 3. Crystal structures of complexes Mn1 and Mn2, with ellipsoids at 50% of probability.

Table 1. Crystal data and structure refinement for complexes Mn1 and Mn2.						
Data	Mn1	Mn2				
Empirical formula	$C_{40}H_{34}MnO_8$	C ₄₀ H ₃₀ Cl ₂ MnO ₈				
CCDC no.	2,373,330	2,373,329				
Formula weight	697.61	764.48				
Temperature/K	293(2)	293(2)				
Crystal system	Monoclinic	Triclinic				
Space group	I2/a	P-1				
a/Å	17.6398(4)	13.4153(4)				
b/Å	9.49159(19)	15.7217(6)				
c/Å	20.7344(5)	17.7435(3)				
α/°	90	91.795(2)				
β/°	102.064(2)	107.422(2)				
γ/°	90	99.234(3)				
V/Å3	3394.87(13)	3511.81(18)				
Z	4	4				
$ ho_{ m calc} { m g/cm^3}$	1.365	1.446				
μ/mm^- 1	3.611	4.912				
F(000)	1452.0	1572.0				
Crystal size/mm ³	0.18 × 0.115 × 0.077	$0.287 \times 0.085 \times 0.021$				
Radiation	Cu K α ($\lambda = 1.54184$)	Cu K α ($\lambda = 1.54184$)				
2⊖ range for data collection/°	10.256 to 140.126	9.8 to 140.146				
Index ranges	$-21 \le h \le 21, -11 \le k \le 8, -25 \le l \le 25$	$-16 \le h \le 16, -19 \le k \le 19, -21 \le l \le 21$				
Reflections collected	37,791	14,321				
Independent reflections	$3225 [R_{sigma} = 0.0237]$	14,321 [R _{sigma} = 0.0571]				
Data/restraints/parameters	3225/30/263	14,321/0/963				
Goodness-of-fit on F ²	1.060	1.032				
Final R indexes [I>= 2σ (I)]	$R_1 = 0.0559$, $wR_2 = 0.1507$	$R_1 = 0.1008, wR_2 = 0.2656$				
Final R indexes [all data]	$R_1 = 0.0610, wR_2 = 0.1550$	$R_1 = 0.1611, wR_2 = 0.3193$				
Largest diff. peak/hole/eÅ ⁻³	0.55/-0.40	1.14/-0.55				

The presence of a chloride atom in HNQ2 has a marked influence over the spatial arrangement of the coordination sphere in Mn2, causing an angular difference of approximately 6° in the axial axis $\angle O2\text{-}Mn\text{-}O5$ (from 175.05° in Mn1 to 169.20° in Mn2) (Table S2). The same 6-degree difference was perceived when comparing the equatorial angle ∠O2-Mn-O6 (102.60° for Mn1 and 95.88° in Mn2). Concerning the C-O bond analysis for the complexes, the carbonyl C1-O1 bond has the shortest length (1.229 Å for Mn1 and 1.221 Å for Mn2), due to a stronger

double bond character that results in weaker donation to the metal center, compared to the C2-O2 (1.279 Å for Mn1 and 1.282 Å for Mn2) and C5-O3 bonds (1.439 Å for Mn1 and 1.419 Å for Mn2) (Table S2).[56] This weaker interaction is corroborated by the Mn-O bond lengths of 2.245/2.268 Å for Mn-O1, 2.119/2.112 Å for Mn-O2, and 2.164/2.150 Å for Mn-O3 (for Mn1/Mn2, respectively).

It should be mentioned that the relatively high R1 value observed for Mn2 (0.1008) arises from the limited quality of the

43, Downloaded from https://chemistry-euope.onlinelibrary.wiley.com/doi/10.1002/slet.202504426 by University Of Sao Paulo - Brazil, Wiley Online Library on [25/11/2025]. See the Terms and Conditions (https://onlinelibrary.wiley.com/terms-and-conditions) on Wiley Online Library for rules of use; OA articles are governed by the applicable Creative Commons License

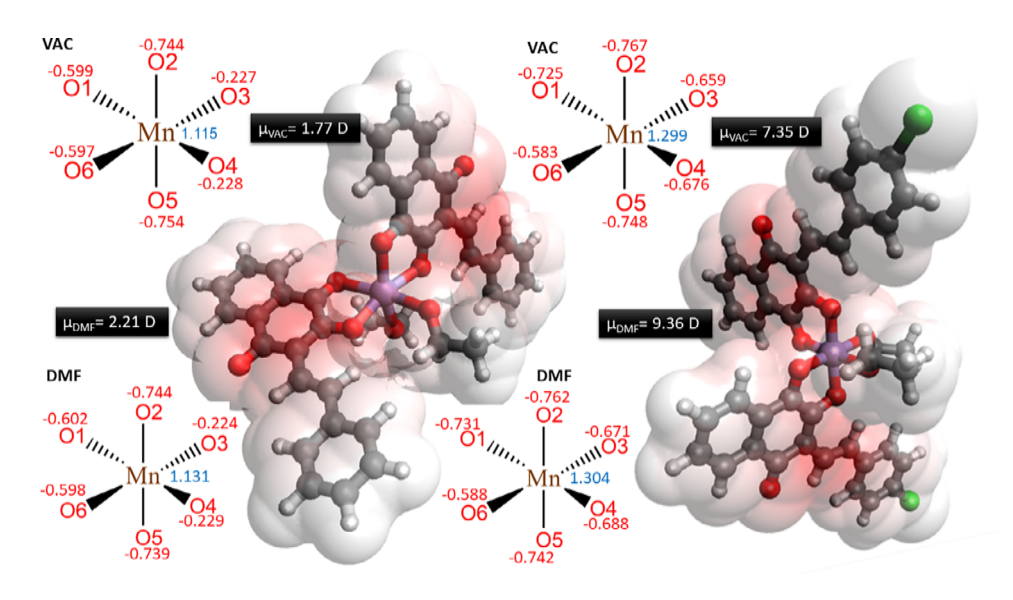


Figure 4. Surface potential maps generated with iso value 0.3 (positive charges are depicted in white, and negative in red), and models for charge distribution, in vacuum and DMF medium ($\varepsilon =$ 37.219), by the single point approach.

single crystal, which was very small, weakly diffracting, and presented disorder. Despite these limitations, the connectivity and overall model are chemically meaningful and consistent with the expected structure.

Following the characterization of **Mn1** and **Mn2**, DFT calculations were carried out to predict the charge distribution and dipole moments of both complexes. Mülliken charges of atoms in the coordination sphere tend to be conserved at approximately -2 (**Mn1**: -2.03 in gas phase and -2.01 in DMF; **Mn2**: -2.86 in gas phase and -2.88 in DMF) (Figure 4). For **Mn2**, there was an increase in charge in the ethanolic oxygens O3 and O4, induced by the polarization of the implicit medium. When comparing the dipole moment module (μ , debye) values calculated for each complex in gas phase and DMF, a proportional 20% difference was also observed (1.77 D versus 2.21 D for **Mn1**; 7.35 D versus 9.36 D for **Mn2**).

Finally, the Gibbs free energy of complex formation for Mn1 and Mn2 in ethanolic medium were calculated. The value of the entropic contribution $T\Delta S_{(Ethanol)}$ was positive (+3.953 kcal mol⁻¹ for Mn1 and + 1.522 kcal mol⁻¹ for Mn2), which was expected due to stability gain caused by the chelate effect in both systems. In terms of enthalpy, the system provided better favoritism for Mn1 $(\Delta H_{(Ethanol)} = -8.750 \text{ kcal mol}^{-1}) \text{ compared to Mn2} (\Delta H_{(Ethanol)})$ $= +4.831 \; \text{kcal mol}^{-1}$), which was corroborated by the analysis of the Gibbs free energy ($\Delta G_{(Ethanol)} = -12.703 \text{ kcal mol}^{-1}$ for Mn1 and + 3.309 kcal mol⁻¹ for Mn2). Considering an experimental error of up to ± 5 kcal mol⁻¹, the formation of both stilbene-quinone complexes could be considered spontaneous, although Mn1 would be around 5 times to more favored. The Gibbs free energy values also corroborate Mn1 remaining in a monoclinic system, which is more symmetrical when compared to the triclinic system found for Mn2. Therefore, considering that the only structural change between HNQ1 and HNQ2 was the para-substitution of hydrogen by chlorine, it is coherent to propose that chlorine contributes to the destabilization of the supramolecular packing of the system.

2.2. Stability in Solution

The stability of the compounds was assessed prior to the biological studies. First, we evaluated the temporal change of the UV–vis spectra obtained in DMSO. No significant changes were observed after 48 h. To obtain more reliable insights about their behavior in aqueous media, the integrity of both complexes was also investigated in PBS (DMSO 1%). Again, no significant changes were observed in their spectra during this period. The same behavior was observed after monitoring their spectra by EPR in DMSO/PBS solutions, confirming their stability during this period (Figures S13 and S14).

2.3. Biological Investigation

After verifying their stability, the cytotoxicity of Mn(II) complexes was investigated against A2780 (Human Ovarian Carcinoma) and A2780-cisR (Human Ovarian Carcinoma Cisplatin Resistant) and MCF-7 (Breast Adenocarcinoma) cells. The free ligands and cisplatin were tested as well, and the results are presented in Table 2. The cytotoxicity of both naphthoguinone ligands has increased upon coordination to a manganese center. Complexes Mn1 and Mn2 were cytotoxic in all cancer cell lines tested, with increased effect against ovarian cancer, highlighting their effect on A2780 cells, with IC_{50} values of 6.89 and 7.58 μM , respectively. These compounds were also tested against noncancerous human lung cells (MRC-5). As observed, the IC₅₀ values obtained for the manganese compounds, 24.91 µM and 16.02 µM, respectively, indicate that Mn1 is approximately 1.6-fold less toxic to the non-cancerous cells than its analogue Mn2. As observed, the free naphthoquinone ligands were non-toxic to these cells at the maximum concentration tested ($IC_{50} > 50$ μM). Subsequently, the selectivity index (SI) was obtained for both complexes. Our findings revealed Mn1 as the most promising candidate, with the best selectivity results on A2780 cells

Table 2. In vitro cytotoxicity (IC₅₀, μ M) results on A2780 (ovarian), A2780-*cis*R (ovarian cisplatin resistant), and MCF-7 (breast) cancer cells and MRC-5 (lung) non-cancerous cells after 48 h of incubation. Data are presented as mean \pm SD of three independent replicates. SI¹ = IC_{50 MRC-5}/IC_{50 A2780}, SI² = IC_{50 MRC-5}/IC_{50 A2780-cis}R and SI³ = IC_{50 MRC-5}/IC_{50 MCF-7}.

Compound	A2780	A2780-cisR	MCF-7	MRC-5	SI1	SI ²	SI ³
Mn1	6.89 ± 0.87	14.05 ± 0.36	30.79 ± 2.05	24.91 ± 1.16	3.6	1.8	0.8
Mn2	7.58 ± 0.37	8.95 ± 1.57	30.29 ± 5.24	16.02 ± 2.33	2.1	1.8	0.5
HNQ1	>25	36.90 ± 2.25	>50	>50	-	>1.3	-
HNQ2	>50	>50	>50	>50	-	-	-
MnCl ₂ •4H ₂ O	>50	>50	>50	>50	-	-	-
cisPt	8.73 ± 0.45	37.02 ± 5.10	13.98 ± 0.40	29.09 ± 0.79	3.3	0.8	2.1

(SI = 3.6). It should be mentioned that Mn1 was more cytotoxic than similar manganese-based complexes reported in the literature. Due to the better results, Mn1 was selected for a deeper biological investigation on A2780 cells.

The morphology of A2780 ovarian cancer cells was studied after 48 h in the presence of Mn1. As presented, significant changes in the shape of the cells were observed, accompanied by non-adherent and spherical cells, mainly at 2 \times IC₅₀ concentration (Figure 5a). These cells were stained, and fluorescence images were taken using a CELENA® S Digital Imaging System. After the treatment with Mn1 at different concentrations ($\frac{1}{2}$ × IC_{50} , IC_{50} , and 2 × IC_{50}), Hoechst 33,258 and PI (propidium iodide) dyes were added. The images were obtained after incubation for 1 h in the dark. As shown, in the absence of Mn1, the ovarian cells remain alive, and only Hoechst fluorescence is observed. On the other hand, PI is used to label dying cells that have a compromised membrane. After adding increasing concentrations of Mn1, the PI fluorescence increased as a consequence of increased dead cell population, characterized by condensed and fragmented chromatin (Figure 5a). This effect was also observed in other cancer cells after treatment with different manganese complexes.^[59,60]

In the next step of our study, the colony formation assay was explored to investigate the antiproliferative potential of Mn1. For this, A2780 cells were treated with Mn1 at $\frac{1}{2}$ IC50, IC50 and $2\times$ IC50 concentrations. The manganese complex was removed after two days, the medium was replaced with fresh medium, and the colonies formed after 10 days were stained with crystal violet, washed, dried, and analyzed using Image J software. $^{[61]}$ As observed in Figure 5b, when compared to the control (untreated cells), the number of colonies decreased in a concentration-dependent manner, highlighting the capacity of Mn1 to reduce the clonogenic survival of A2780 cells.

To investigate whether ROS plays a crucial role in cell death, intracellular ROS levels were examined in A2780 ovarian cancer cells after treatment with Mn1. As reported, ROS are highly unstable and short-lived molecules generated during cellular processes, and their excessive accumulation can damage cellular organelles, leading to oxidative cell death. Consequently, the anticancer activity of metal-based compounds may be affected by the excessive production of these species. Although there are several manganese complexes reported as ROS inducers, our results revealed that the presence of Mn1 did not induce

significant changes in ROS levels at the concentrations tested, compared to the negative control, suggesting that the cell death mechanism induced by this complex is not related to oxidative stress (Figure S15).^[44,59]

2.4. DNA-Interacting Studies

DNA remains the primary target for metal-based compounds in medicinal inorganic chemistry. Manganese- and other metal-based complexes can bind to DNA in different ways. [65–67] First, covalent bonds can occur with nucleophiles involving nitrogen or oxygen atoms of the nucleobases. In addition, noncovalent bonds arise from intercalation between base pairs, insertion, through electrostatic contacts with the sugar-phosphate backbone, or via groove binding, where the molecule can interact through minor or major pockets. Here, we use circular dichroism (CD) and dye-displacement fluorescence experiments to obtain better insights about the interaction between Mn1 and DNA. CT-DNA (calf thymus) was employed in all experiments. The DNA concentration was measured using a spectrophotometer at 260 nm, based on the nucleobase molar absorptivity of 6600 M⁻¹ cm⁻¹.

Circular dichroism is a suitable spectroscopic technique used to study structural changes in biomolecules. CD bands observed for B-DNA, the most common studied DNA form, are close to 275 nm (positive) and 245 nm (negative), and are typical of base stacking and helicity (right-handed twist), respectively. [68,69] The CT-DNA solution was incubated with increased concentrations of Mn1 for 24 h at 37 °C. As observed, no significant changes were detected from the CD spectra. As both bands remained unchanged during the analyses, covalent binding was excluded. Our results revealed that Mn1 is unable to disturb the second structure of the biomolecule, suggesting that interactions occur via noncovalent contacts (Figure 6a). [70,71]

To study further the interactions between Mn1 and DNA, competitive binding with ethidium bromide (EB) and Hoechst 33258 was conducted. These DNA-interacting dyes emit fluorescence at 610 nm (EB) and 460 nm (Hoechst) when bound to biomolecules upon excitation at 540 and 340 nm, respectively. Whereas EB intercalates between the DNA base pairs, Hoechst is a groove-binding agent that interacts via the minor groove pocket. All fluorescence emission spectra of Mn1 with

43, Downloaded from https://chemistry-cuope.onlinelibrary.wiley.com/doi/10.1002/slct.202504426 by University Of Sao Paulo - Brazil, Wiley Online Library on [25/11/2025]. See the Terms and Conditions (https://onlinelibrary.wiley.com/ems-and-conditions) on Wiley Online Library for rules of use; OA archies are governed by the apaplicable Creative Commons License

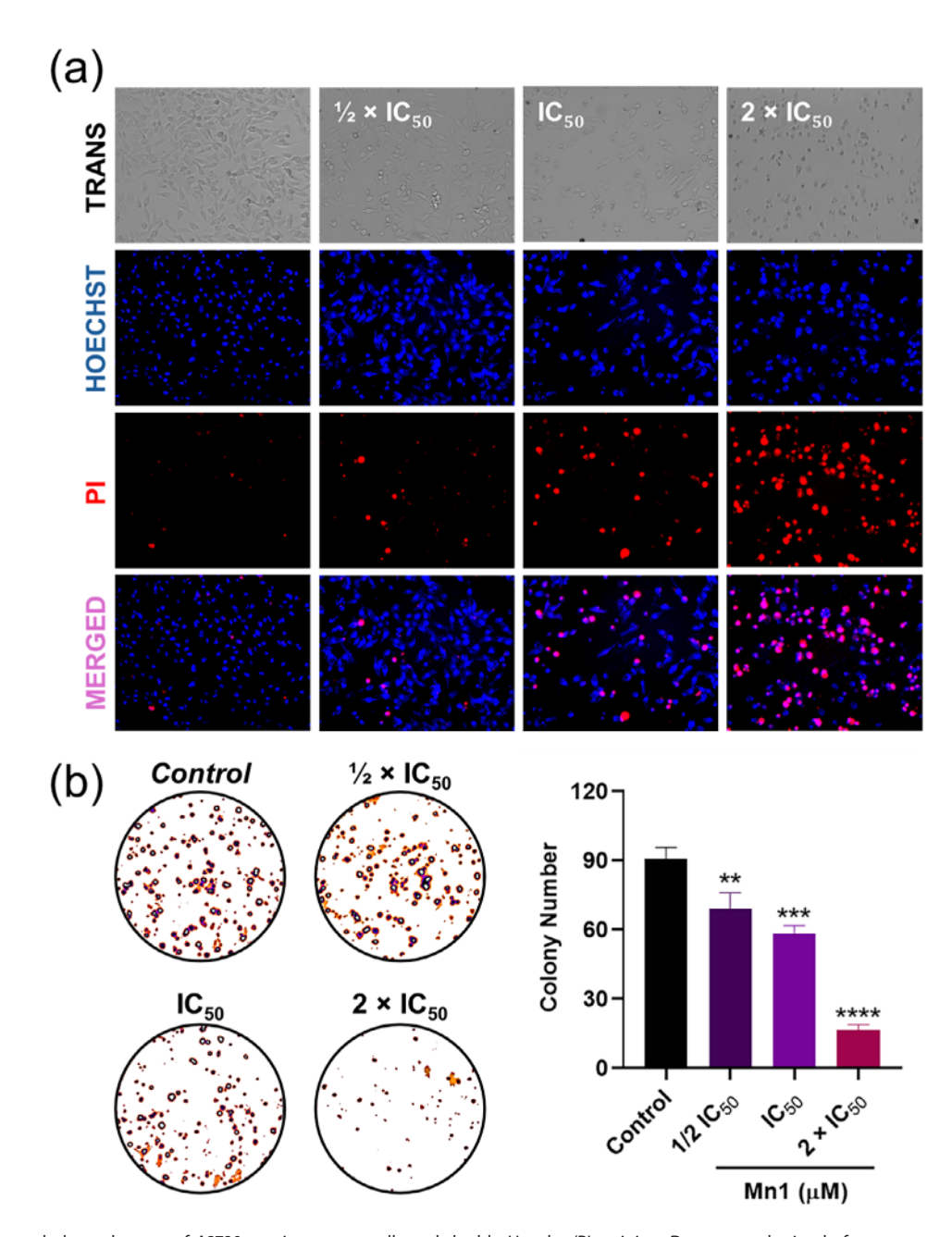


Figure 5. a) Cell morphology changes of A2780 ovarian cancer cells and double Hoechst/PI staining. Data were obtained after treatment with Mn1 for 48 h at $\frac{1}{5}$ IC₅₀, IC₅₀, and 2 × IC₅₀ concentrations. The images were taken using a CELENA® S Digital Imaging System (Logos Biosystems) at 10 × zoom. b) Representative colony formation images (left), and quantitative data representing the colony number (right) of A2780 cells in the presence of Mn1 at $\frac{1}{2}$ IC₅₀, IC_{50} , and $2 \times IC_{50}$. DMSO vehicle (0.5% v/v) was used in the negative control. Data are expressed as mean \pm SD of three independent measurements. The statistical analysis was performed with one-way ANOVA followed by Dunnett's test (**p < 0.01, ***p < 0.001, and ****p < 0.0001).

both DNA:dye adducts are presented in Figure 6 and in the Supporting Information (Figure S15). As presented, a fluorescence quenching was observed when Mn1 was added to both DNA:EB and DNA:Hoechst solutions, suggesting a displacement of EB and Hoechst from the biomolecule (Figure 6b,c).

To understand deeper whether the possible interaction of Mn1 occurs via intercalation or groove binding, several parameters were investigated at different temperatures, such as the Stern–Volmer (K_{SV}), bimolecular quenching rate (k_q), and binding (K_b) constants (Table 1). The results obtained for DNA:EB revealed a quenching of 50%, with a K_{SV} in a range of 10^4 M $^{-1}$, which is close to obtained for different manganese complexes.^[72] Despite the lower K_b value than observed for EB ($K_b = 10^6 \text{ M}^{-1}$), [73] the binding constant for Mn1 is higher than those reported in the literature^[74] The partial quenching of fluorescence could be associated with the formation of a ternary complex DNA:EB-Mn1, where the presence of a neutral manganese compound changes the structure of DNA:EB but is not enough to displace the dye. Therefore, our results indicate that Mn1 did not act as an intercalating agent. As mentioned, the same experiment was conducted with Hoechst 33,258. Different from observed for DNA:EB, the results obtained for DNA:Hoechst system clearly

43, Downloaded from https://chemistry-cuope.onlinelibrary.wiley.com/doi/10.1002/slct.202504426 by University Of Sao Paulo - Brazil, Wiley Online Library on [25/11/2025]. See the Terms and Conditions (https://onlinelibrary.wiley.com/ems-and-conditions) on Wiley Online Library for rules of use; OA archies are governed by the apaplicable Creative Commons License

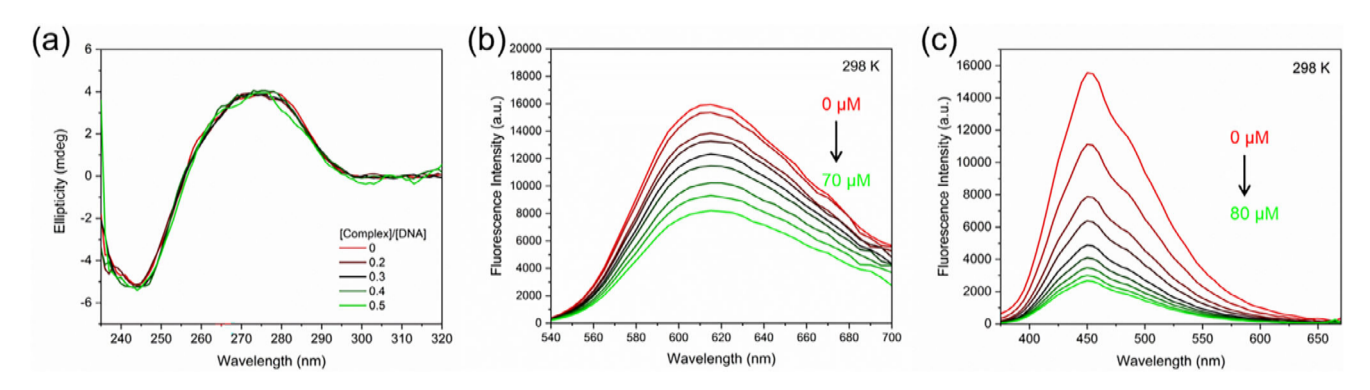


Figure 6. Binding studies with DNA: a) CD spectra of CT–DNA (100 μ M) in the absence and presence of Mn1 at different concentrations (20–50 μ M). b) Fluorescence emission spectra of the DNA–EB complex in the absence and presence of increasing amounts of Mn1, [EB] = 70 μ M, [DNA] = 70 μ M, [Complex] = 0–70 μ M, λ exc = 540 nm. c) Fluorescence emission spectra of the DNA–Hoechst complex in the absence and presence of increasing amounts of Mn1, [Hoechst] = 5 μ M, [DNA] = 80 μ M, [Complex] = 0–80 μ M, λ exc = 340 nm.

Table 3. DNA-binding properties of Mn1 by fluorescence analysis. K_{SV} : determined by Stern–Volmer quenching constant; k_q : determined by the K_{SV}/τ_0 ratio, where $\tau_0=23$ ns (EB:DNA), 5 ns (Hoechst:DNA). K_b : determined by the modified Stern–Volmer equation.

-			•	·		
	<i>T</i> (K)	Q (%)	$K_{SV} \ (\times \ 10^4, \ M^{-1})$	$k_q~(\times~10^{12},~M^{-1}~s^{-1})$	$K_{\rm b}~(\times~10^4,~{\rm M}^{-1})$	ΔG (KJ/mol)
DNA:EB	298	49	1.20 ± 0.03	0.52 ± 0.01	4.90 ± 0.05	-26.76
-	303	50	1.23 ± 0.04	0.54 ± 0.02	1.21 ± 0.09	-23.69
-	310	51	1.28 ± 0.01	0.56 ± 0.07	1.20 ± 0.03	-24.21
DNA:Hoechst	298	83	6.44 ± 0.09	12.89 ± 0.18	4.68 ± 0.03	-26.64
_	303	82	6.12 ± 0.07	12.23 ± 0.13	4.67 ± 0.05	-27.08
_	310	81	5.94 ± 0.06	11.87 ± 0.12	4.59 ± 0.07	-27.66

indicate Mn1 as minor groove binder. Although the lower K_b constant, the manganese compound caused a strong suppression of fluorescence, around 80%. In this case, the K_{SV} was fourfold higher than observed for EB system, and decreased with increasing the temperature, suggesting a static mechanism.^[75] This mechanism is also supported by the k_q constant. As presented in Table 3, these values are higher than maximum value possible for a dynamic mechanism ($\sim 10^{10}~{\rm M}^{-1}~{\rm s}^{-1}$). Finally, the thermodynamic parameters were also studied. For both systems, the free energy obtained by equation $\Delta G = -RTInK_b$ was in a range between -23.69 and -27.66 indicating a spontaneous process. Furthermore, ΔH and ΔS obtained for DNA:Hoechst system in a presence of Mn1, -1.32 KJ/mol and + 84.98 J/mol, respectively, indicate an exothermic process due a combination of van der Waals and hydrogen bonds interactions, and the releasing of water molecules in a groove pocket due the hydrophobic effect. Therefore, our investigation revealed that interaction between Mn1 and DNA occurs via groove binding, which is predominantly entropically driven.^[76] This result is in agreement with circular dichroism data.

cis configuration of the ethanol ligands and the distorted octahedral geometry around the Mn(II) center. The electrochemical behavior of Mn1 and Mn2 was investigated by cyclic voltammetry, which showed the Mn^{II}/Mn^{III} and Mn^{III}/Mn^{IV} one-electron redox processes. The Mülliken charges around the Mn(II) ion and dipole moments of both complexes were calculated by DFT, as well as the enthalpy, entropy, and Gibbs energy of complex formation, which suggested that Mn1 is more favored than Mn2. Both complexes were cytotoxic against several cancer cell lines, highlighting the effect of Mn1 on A2780 ovarian cancer cells. This compound was able to alter morphology and inhibit colony formation in A2780 cells. Although it does not act through oxidative stress, Mn1 interacts with DNA via the minor groove pocket, which may be associated with its cytotoxic properties. These findings may be useful for the development of more cytotoxic and selective manganese-based quinone compounds against ovarian cancer.

coordinate to the Mn(II) center as anionic O,O-bidentate ligands.

Elemental analysis and conductance measurements suggested

the general formula [Mn(HNQ)2(EtOH)2], which was later con-

firmed by single-crystal X-ray crystallography together with the

3. Conclusion

Two novel Mn(II) coordination compounds derived from stilbene-quinone ligands were obtained from the reaction of MnCl₂•4H₂O with **HNQ1** and **HNQ2**. FTIR and UV–vis spectroscopy analyses indicated that the stilbene-quinone hybrids

4. Experimental Section

Material and Instrumental Details: The reagents and solvents used in this work were purchased from Merck, Sigma-Aldrich, Vetec, Fluka, Tedia, or Carlo Erba, and were used as received with no



further purification. Purification of the ligands was carried out by flash chromatography on Tedia silica gel with granulation 0.040-0.063 mm. Reactions were monitored by analytical thin-layer chromatography (TLC) on 0.25 mm silica gel 60 F254 plates using EtOAc:hexane (30:70) as eluent and visualized under UV light (254 or 365 nm). Infrared spectra (IR) were recorded on KBr pellets with 32 scans set on a Shimadzu IRAffinity-1 spectrometer in the region from 4000 to 400 cm⁻¹ with 4 cm⁻¹ resolution. UV-vis spectra were recorded using a Shimadzu UV-Vis 2600 spectrophotometer with a 1.0 cm quartz cell. Measurements were carried out in DMSO from 200 to 800 nm, and molar absorptivity coefficients (ε) were determined by applying the Lambert-Beer law. Nuclear magnetic resonance (NMR) spectra were acquired in deuterated chloroform (CDCl₃) in a Varian MR-400 instrument at 293 K. Chemical shifts (δ) are reported in parts per million (ppm) relative to tetramethylsilane (TMS) and referenced to the ¹H or ¹³C resonance of residual CHCl3. The NMR data are represented as follows: chemical shift (ppm), multiplicity (s = singlet, d = doublet, t = triplet, dd = doublet of doublets, td = triplet of doublets, m = multiplet), coupling constant in Hertz (Hz), and integration. The EPR measurements were performed in a Bruker model ELEXSYS electron paramagnetic resonance microwave bridge ESP 380-1010. The samples were measured in DMSO solution at 295 K. Conductance measurements were recorded using an Ion DDS-12DW electrical conductivity meter using DMF medium at 1.0×10^{-3} mol L⁻¹. Cyclic voltammetry measurements were recorded at room temperature in CH₂Cl₂ with 0.1 mol L⁻¹ tetrabutylammonium perchlorate (TBACIO₄), using an Autolab PGSTAT potentiostat/galvanostat equipped with a glassy carbon working electrode, a platinum auxiliary electrode, and a reference Ag/AgCl electrode.

Synthesis of the stilbene-quinone derivatives (HNQ1 and HNQ2): Stilbene-quinone hybrids HNQ1 and HNQ2 were prepared as previously reported. A mixture of 3-iodolawsone (300 mg, 1 mmol), the corresponding styrene derivative (1 mmol), NaOH (120 mg, 3 mmol), and [Pd(OAc)₂] (22.4 mg, 10 mol%) in PEG-400 (8 g) was magnetically stirred at 90 °C for 15 minutes. The mixture was diluted with ethyl acetate (40 mL) and filtered through a plug of celite. The filtrate was acidified with 25% aq. H₃PO₄ (25 mL), and the organic phase was washed with brine (3 x 50 mL), dried over anhydrous Na₂SO₄, and concentrated under reduced pressure. The resulting dark residue was purified by flash chromatography on silica gel using a mixture of EtOAc/Hexane (5:95) as eluent, affording HNQ1 and HNQ2 as red solids.

2-Hydroxy-3-styryl-1,4-naphthoquinone (HNQ1): Red solid, 220 mg, 80% yield. MP (160–161 °C). UV–vis λ max (DMSO)/nm (ε /L mol-1 cm-1): 312 (47852), 382 (3580), 400 (4285), 474 (8794). FTIR [ν max/cm⁻¹] 3312 (OH), 1647 (C=O), 1590 (C=O), 1375 (C=C), 1263 (C-O). 1 H NMR (400 MHz, CDCl $_3$) δ 8.14 (d, J = 7.7 Hz, 1H, H8), 8.06 (d, J = 7.5 Hz, 1H, Ar-H, H5), 7.94 (d, J = 16.7 Hz, 1H, H7'), 7.74 (td, J = 7.6, 1.2 Hz, 1H, H7), 7.67 (td, J = 7.5, 1.2 Hz, 1H, Ar-H, H6), 7.57 (d, J = 7.4 Hz, 2H, H2' and H6'), 7.37 (d, J = 16.8 Hz, 1H, H8'), 7.40 – 7.33 (m, 2H, H3' and H5'), 7.28 (m, 1H, H4'). 13 C NMR (101 MHz, CDCl $_3$) δ 184.2, 181.1, 151.8, 139.4, 137.9, 135.1, 133.3, 132.8, 129.6, 128.8, 128.8, 127.3, 127.2, 126.2, 118.8, 117.5.

2-Hydroxy-3-(4-chlorostyryl)-1,4-naphthoquinone (HNQ2): Red solid, 193 mg, 63% yield. MP (190 °C). UV-Vis λ_{max} (DMSO)/nm (ε /L mol⁻¹ cm⁻¹): 316 (37004), 386 (4712), 405 (5141), 469 (6727). FTIR [ν_{max} /cm⁻¹] 3260 (OH), 1666 (C=O), 1592 (C=O), 1349 (C=C), 1275 (C-O). ¹H NMR (400 MHz, CDCl₃) δ 8.17 (dd, J = 7.6, 0.9 Hz, 1H, H8), 8.10 (dd, J = 7.6, 1.0 Hz, 1H, H5), 7.91 (d, J = 16.7 Hz, 1H, H7), 7.78 (td, J = 7.6, 1.4 Hz, 1H, H7), 7.71 (td, J = 7.5, 1.3 Hz, 1H, H6), 7.52 (d, J = 8.4 Hz, 2H, H2' and H6'), 7.36 (d, J = 16.7 Hz, 1H, H8'), 7.34 (d, J = 8.5 Hz, 2H, H3' and H5'). ¹³C {¹H} NMR (101 MHz, CDCl₃) δ 184.0,

180.9, 151.8, 137.8, 136.2, 135.1, 134.3, 133.3, 132.6, 129.5, 128.9, 128.3, 127.2, 126.1, 118.3, 117.9.

Synthesis of Mn(II) complexes (Mn1 and Mn2): A mixture of the corresponding ligand (HNQ1 or HNQ2, 0.50 mmol) and triethylamine (140 μL, 1.0 mmol) was dissolved in EtOH (10 mL), resulting in a dark purple solution. This deprotonated ligand solution was slowly added to a solution of MnCl₂•4H₂O (50 mg, 0.25 mmol) in absolute EtOH (5 mL) and left without stirring for 24 h at room temperature at sea level. The resulting dark blue crystals were vacuum filtered in a sintered funnel, washed with cold absolute EtOH, and left to dry in a desiccator under vacuum.

[Mn(NQ1)₂(EtOH)₂] (Mn1): Dark-blue crystals, 148 mg, 85% yield. Elemental analysis for [C₄₀H₃₄MnO₈], in percentage: C, 69.01 (calc. 68.87); H, 5.02 (calc. 4.91). $\Lambda_{\rm M}=26.7~\Omega^{-1}~{\rm cm^2~mol^{-1}}$, in 1.0 mM DMF solution. UV–vis $\lambda_{\rm max}$ (DMSO)/nm (ε /L mol⁻¹ cm⁻¹): 336 (22000), 380 (42800), 574 (4000). FTIR [$\nu_{\rm max}$ /cm⁻¹]: 3257 (OH), 1584 (C=O), 1533 (C=O), 1363 (C=C), 1294 (C-O), 487 (Mn-O).

[Mn(NQ2)₂(EtOH)₂] (Mn2): Dark-blue crystals, 153 mg, 80% yield. Elemental analysis for [C₄₀H₃₂Cl₂MnO₈]•0.02 EtOH, in percentage: C, 63.08 (calc. 62.68); H, 4.63 (calc. 4.21). $\Lambda_{\rm M}=31.6~\Omega^{-1}~{\rm cm^2~mol^{-1}}$, in 1.0 mM DMF solution. UV-vis $\lambda_{\rm max}$ (DMSO)/nm (ε /L mol⁻¹ cm⁻¹): 334 (23600), 386 (55600), 568 (4920). FTIR [$\nu_{\rm max}$ /cm⁻¹]: 3203 (OH), 1584 (C=O), 1532 (C=O), 1364 (C=C), 1295 (C-O), 500 (Mn-O).

X-ray crystallography: Complexes Mn1 and Mn2 were crystallized from the ethanolic reaction mixture overnight. The measurements of single crystals by X-ray diffraction were performed on Rigaku Synergy-S diffractometer with Cu/Mo K α radiation. Cell refinements were carried out using the CrysAlisPro software, and the structures were obtained by the intrinsic phasing method using the SHELXT program. The Gaussian method was used for the absorption corrections. Table and structure representations were generated by OLEX2 and MERCURY, and MERCURY, crystallographic data for the reported structures have been deposited with the Cambridge Crystallographic Data Centre (CCDC) under the deposition numbers 2373329 and 2373330. These data can be obtained free of charge via the CCDC website or e-mail: deposit@ccdc.cam.ac.uk. The deposited data include atomic coordinates, bond lengths and angles, torsional angles, and displacement parameters.

Computational approaches: Molecular calculations were performed with the software Gaussian 16 Rev. C.01. [80] Geometry optimization was carried out considering the gaseous phase at the Density Functional Theory (DFT) level using the hybrid functional B3LYP^[81-83] with base set function 6-31G(d).^[84] To evaluate the solvent effect of implicit medium, the treatment method IEF-PCM^[85] was used at a single point, adjusting the dielectric constant for the solvent ethanol ($\varepsilon=24.8520$), and the $\Delta E_{(\text{ethanol})}$ value was calculated to sum the gas phase energy. Normal IR vibration modes and reactional free energy ($\Delta G_{(ethanol)}$) and enthalpy ($\Delta H_{(ethanol)}$) for the complexes Mn1 and Mn2 were calculated considering high spin with zero charges. Since the reaction is not monomolecular, the standard state correction adds the value of + 3.78 kcal mol⁻¹ to the $\Delta G_{(ethanol)}$ value. With the proposal to analyze the charges of the coordination sphere and calculate the dipole moment module, DMF medium was considered ($\varepsilon = 37.219$).

Stability studies: The stability of the compounds was assessed prior to the biological studies. UV–vis spectra of these species were recorded in DMSO and PBS buffer solutions containing DMSO 1% at 0, 24, and 48 h. Also, DMSO/PBS (90:10) solutions were prepared, and the EPR spectra were monitored at 0, 24, and 48 h. The EPR measurements were performed at the University of São Paulo (USP), São Carlos, Brazil.

Cell culture: The manganese compounds and free ligands were tested against human ovarian cancer cells A2780 (ECACC



93112519), cisplatin-resistant human ovarian cancer cells A2780-cisR (ECACC 93112517), breast cancer cells MCF-7 (ATCC HTB-22), and non-cancerous lung cells MRC-5 (ATCC CCL-171). The cells were routinely maintained with Roswell Park Memorial Institute 1640 medium (RPMI 1640, for A2780, A2780-cisR, and MCF-7) or Dulbecco's modified Eagle's medium (DMEM, for MRC-5) supplemented with 10% fetal bovine serum (FBS), at 37 °C in a humidified 5% CO₂ atmosphere. The cells were obtained from Rio de Janeiro Cell Bank (BCRJ). Cell culture media and FBS were obtained from Vitrocell and Gibco, respectively.

In vitro cytotoxicity: The cytotoxic activity of the compounds was investigated via 3-(4,5-dimethylthiazol-2-yl)-2,5diphenyltetrazolium bromide (MTT) assay. [86] Cells (1.0 \times 10 4 cells/well) were seeded in 96-well plates (150 µL/well) and incubated for 24 h (37 °C, 5% CO_2). After this period, 0.75 μL of the compounds were added at 8 different concentrations (0.024 to 50 μmol L⁻¹), containing a final concentration of 0.5% DMSO, and the plates were kept in the incubator for 48 h. After the incubation, 50 µL of MTT (1.0 mg/mL in PBS) was added to each well and the cells were incubated again for 4 h. The medium was removed, and the formazan crystals formed were solubilized by adding 150 µL of DMSO. The absorbance was measured using a microplate spectrophotometer (Epoch, BioTek) at 540 nm. All compounds were tested in three independent experiments performed in triplicate. Cisplatin drug, the free ligands and MnCl₂ were also tested, and DMSO was used as the negative control (0.5%). From the absorbance, IC50 (concentration required to inhibit cell viability by 50%) was calculated using GraphPad Prism 8.0.2 software and reported as mean \pm standard deviation.

Cell morphology and Hoechst/PI double staining: For morphological analysis, A2780 cancer cells (1.0 \times 10^4 cells/well) were seeded in a 96-well plate (150 $\mu L/\text{well})$ and then incubated at 37 °C in 5% CO $_2$ for 24 h. After this period, the cells were treated with Mn1 at $\frac{1}{2} \times IC_{50}$, IC $_{50}$, and 2 \times IC $_{50}$ concentrations (3.50–13.80 μM). After 48 h of treatment, the images were captured using a CELENA S Digital Imaging System (Logos Biosystems). For the double staining, the cells were incubated with Hoechst 33258 and propidium iodide (PI) for 1 h in the dark before imaging.

Clonogenic survival assay: Cells (0.6 \times 10³ cells/well) were seeded in a 6-well plate (2 mL/well) and then incubated at 37 °C in 5% CO₂ for 24 h. After this period, the cells were treated with Mn1 at $\frac{1}{2} \times IC_{50}$, IC_{50} , and 2 \times IC_{50} concentrations (3.50–13.80 μ M) and incubated for an additional 48 h. Then, the culture medium was replaced with fresh medium, and the plates were incubated for an additional 10 days. After this period, the culture medium was removed, and the colonies formed were washed, fixed, and then stained. Furthermore, the plates were washed with water and dried at 25 °C. The experiment was performed in triplicate. The colony number was calculated using ImageJ software as reported. [87]

ROS detection: A2780 cells (2 \times 10 5 cells/well) were seeded in a 24-well plate (1 mL/well) and then incubated at 37 $^{\circ}$ C in 5% CO₂ for 24 h. After this period, the cells were treated with Mn1 at $1/8 \times IC_{50}$, $\frac{1}{4} IC_{50}$, and $\frac{1}{2} \times IC_{50}$ concentrations (0.87–3.50 µM) and incubated for an additional 6 h. After treatment, the cells were incubated with 10 μ M 2',7'-dichlorofluorescein diacetate (H₂DCFDA) in RPMI in the dark at 37 °C for 30 min. The medium was removed, and the cells were washed twice with ice-cold PBS. After removing the PBS, 150 µL of radioimmunoprecipitation assay (RIPA) buffer was added to each well. The plate was incubated on ice for 5 min, and then the cell lysate was collected and centrifuged at 1500 rpm for 5 min. The supernatant of each sample was added, in triplicate, to a 96-well clear-bottom black plate and analyzed on the fluorimeter (Synergy/H1-Biotek) at an excitation wavelength of 485 nm and emission wavelength of 530 nm. The experiment was carried out in triplicate.

4.1. DNA Interacting-Studies

CT-DNA preparation. CT-DNA (Calf Thymus deoxyribonucleic acid sodium salt, Sigma-Aldrich) was prepared in 10 mL of Tris-HCl buffer (0.5 mM Tris-base, 4.5 mM Tris-HCl, and 50 mM NaCl; pH 7.4). The CT-DNA concentration was determined by UV-vis, by using the absorbance and molar absorptivity of DNA at 260 nm ($\varepsilon=6600$ cm⁻¹ mol⁻¹ L) and the optical path length (b = 1 cm), according to the Lambert–Beer law: $A_{260}=\varepsilon\times b\times c$.

Dye displacement assays: Ethidium bromide: A solution of CT-DNA (70 µM) was pre-incubated with EB (70 µM) in Tris-HCl buffer (pH 7.4) for 1 h at 310 K, to allow full interaction of the dye with the biomolecule. Increasing amounts of Mn1 (0-70 µM) were subsequently added to the DNA samples, followed by incubation for 24 h. Fluorescence spectra were registered from 370 to 700 nm at 298 K upon excitation at 540 nm using a Synergy/H1-Biotek fluorimeter. Hoechst 33,258: A solution of CT-DNA (80 µM) was pre-incubated with Hoechst 33,258 (5 µM) in Tris-HCl buffer (pH 7.4) for 1 h at 310 K, to allow full interaction of the dye with the biomolecule. Increasing amounts of Mn1 (0–80 μ M) were subsequently added to the DNA samples, followed by incubation for 24 h. Fluorescence spectra were registered from 370 to 700 nm at 298 K upon excitation at 340 nm using a Synergy/H1-Biotek fluorimeter. For both experiments, the Stern–Volmer quenching (K_{SV}) and bimolecular quenching rate (k_q) constants were calculated according to the DNA:dye fluorescence quenching using a plot of F_0/F versus [Mn1] and a ratio of $K_{SV}/$ au_0 , where the au_0 denotes the fluorescence lifetime of DNA:dye (EB = 23.0 ns; Hoechst = 5.0 ns), respectively. Binding (K_b) constant and thermodynamic parameters were also obtained.

Circular dichroism: CT-DNA (100 μ M) and Mn1 (20–50 μ M) solutions were prepared in Tris-HCl buffer (pH 7.4) to achieve [complex]/[CT-DNA] molar ratios ranging from 0.2 to 0.5. The DMSO percentage was maintained at 10%. Additionally, a solution containing only CT-DNA was prepared as a control. The samples were incubated at 310 K for 24 h. Spectra were recorded between 240 and 400 nm at 200 nm min⁻¹ by using a JASCO J815 spectropolarimeter and five accumulations per measurement, at 298 K. The nitrogen flow was kept constant throughout the measurements.

Acknowledgments

The authors are grateful to FAPERJ (E26/010.002261/2019, E-26/210.070/2022) and FAPESP (2017/15850–0, 2017/01189–0). M.V.P.-M. acknowledges the São Paulo State Research Foundation (FAPESP, Grant 2021/01787–0). This work was carried out with the support of the Coordination of Improvement of Higher Education Personnel Brazil (CAPES) - Code of Financing 001.

The Article Processing Charge for the publication of this research was funded by the Coordenação de Aperfeiçoamento de Pessoal de Nível Superior - Brasil (CAPES) (ROR identifier: 00x0ma614).

Conflict of Interests

The authors declare no conflict of interest.

Data Availability Statement

The data that support the findings of this study are available from the corresponding author upon reasonable request.

Keywords: Bioinorganic chemistry · DNA · Manganese · Metal Complex · Naphthoquinone

- [1] L. I. López López, S. D. Nery Flores, S. Y. Silva Belmares, A. Sáenz Galindo, *Vitae* **2014**, *21*, 248–258.
- [2] M. M. Rahman, M. R. Islam, S. Akash, S. Shohag, L. Ahmed, F. A. Supti, A. Rauf, A. S. M. Aljohani, W. Al Abdulmonem, A. A. Khalil, R. Sharma, M. Thiruvengadam, *Chem.-Biol. Interact.* 2022, 368, 110198, https://doi.org/10. 1016/j.cbi.2022.110198.
- [3] C. G. S. Lima, A. S. Souza, F. P. Pauli, R. C. B. Ribeiro, A. A. Borges, P. G. Ferreira, F. C. Silva, V. F. Ferreira, L. S. M. Forezi, *Curr. Org. Chem.* 2021, 25, 2156–2174, https://doi.org/10.2174/1385272825666210811121450.
- [4] Y. Kumagai, Y. Shinkai, T. Miura, A. K. Cho, Annu. Rev. Pharmacol. Toxicol. 2012, 52, 221–247, https://doi.org/10.1146/annurev-pharmtox-010611-134517
- [5] L. O. Klotz, X. Hou, C. Jacob, Molecules 2014, 19, 14902–14918, https://doi. org/10.3390/molecules190914902.
- [6] J. L. Bolton, T. Dunlap, Chem. Chemical research in toxicology 2017, 30, 13–37, https://doi.org/10.1021/acs.chemrestox.6b00256.
- [7] F. C. Demidoff, M. N. Rennó, C. D. Netto, in Studies in Natural Products Chemistry, Elsevier, Amsterdam 2022, 45–70.
- [8] D. O. Futuro, P. G. Ferreira, C. D. Nicoletti, L. P. Borba-Santos, F. C. D. Silva, S. Rozental, V. F. Ferreira, Anais da Academia Brasileira de Ciências 2018, 90, 1187–1214.
- [9] W. Wang, C. T. Chang, Q. Zhang, ChemistrySelect 2022, 7, e202203330, https://doi.org/10.1002/slct.202203330.
- [10] G. Navarro-Tovar, S. Vega-Rodríguez, E. Leyva, S. Loredo-Carrillo, D. Loera, L. I. López-López, *Pharmaceuticals* 2023, 16, 496, https://doi.org/10.3390/ph16040496.
- [11] R. Rani, K. Sethi, S. Gupta, R. S. Varma, R. Kumar, Curr. Top. Med. Chem. 2022, 22, 2087–2105, https://doi.org/10.2174/1568026622666220912101332.
- [12] E. Ortiz-Pérez, G. Rivera, C. O. Salas, J. J. Zarate-Ramos, O. S. Trofymchuk, L. Hernandez-Soberanis, J. D. Perales-Flores, K. Vázquez, Curr. Top. Med. Chem. 2021, 21, 2046–2069, https://doi.org/10.2174/1568026621666210915121348.
- [13] A. K. Jordão, M. D. Vargas, A. C. Pinto, F. D. C. Silva, V. F. Ferreira, RSC Adv. 2015, 5, 67909–67943.
- [14] V. Allam, S. Jeedi, V. Allam, S. Nerella, B. Gavaji, ChemistrySelect 2024, 9, e202303270, https://doi.org/10.1002/slct.202303270.
- [15] H. Kamil Zaidan, H. H. Jasim Al-Khafaji, F. Al-dolaimy, S. Abed Hussein, R. Otbah Farqad, D. Thabit, A. Talib Kareem, M. F. Ramadan, S. A. Hamood, A. H. Alawadi, A. Alsaalamy, Chem. Biodiversity 2024, 21, e202301777, https://doi.org/10.1002/cbdv.202301777.
- [16] G. J. Kapadia, G. S. Rao, R. Sridhar, E. Ichiishi, M. Takasaki, N. Suzuki, T. Konoshima, A. Iida, H. Tokuda, Anti-Cancer Agents Med. Chem. 2013, 13, 1500–1507.
- [17] L. Rubini-Dias, T. V. A. Fernandes, M. P. Souza, D. Hottz, A. T. Arruda, A. D. A. Borges, G. Ouverney, F. D. C. Silva, L. D. S. M. Forezi, G. Limaverde-Sousa, B. K. Robbs, *Biomedicines* 2024, 12, 2916, https://doi.org/10.3390/biomedicines12122916.
- [18] F. M. Ottoni, E. R. Gomes, R. M. Pádua, M. C. Oliveira, I. T. Silva, R. J. Alves, *Bioorg. Med. Chem. Lett.* 2020, 30, 126817, https://doi.org/10.1016/j.bmcl.2019.126817.
- [19] R. A. Grandis, K. M. Oliveira, A. P. M. Guedes, P. W. S. Santos, A. F. Aissa, A. A. Batista, F. R. Pavan, Front. Oncol. 2021, 11, 682968, https://doi.org/ 10.3389/fonc.2021.682968.
- [20] H. Hussain, K. Krohn, V. U. Ahmad, G. A. Miana, I. R. Green, Arkivoc 2007, 2007, 145–171.
- [21] F. Epifano, S. Genovese, S. Fiorito, V. Mathieu, R. Kiss, *Phytochem. Rev.* 2014, 13, 37–49, https://doi.org/10.1007/s11101-013-9289-1.
- [22] H. Hussain, I. R. Green, Expert Opin. Ther. Pat. 2017, 27, 1111–1121, https://doi.org/10.1080/13543776.2017.1339792.
- [23] S. E. Loredo-Carrillo, E. Leyva, L. I. López-López, G. Navarro-Tovar, D. Loera, S. Vega-Rodríguez, Curr. Org. Chem. 2024, 28, 1118–1141, https://doi.org/10.2174/0113852728299375240405053207.
- [24] I. K. Srivastava, H. Rottenberg, A. B. Vaidya, J. Biol. Chem. 1997, 272, 3961–3966, https://doi.org/10.1074/jbc.272.7.3961.
- [25] V. A. Balta, D. Stiffler, A. Sayeed, A. K. Tripathi, R. Elahi, G. Mlambo, R. P. Bakshi, A. G. Dziedzic, A. E. Jedlicka, E. Nenortas, K. Romero-Rodriguez, M. A. Canonizado, A. Mann, A. Owen, D. J. Sullivan, S. T. Prigge, P.

- Sinnis, T. A. Shapiro, *Nat. Commun.* **2023**, *14*, 6415, https://doi.org/10.1038/s41467-023-42030-x.
- [26] N. N. Sharma, A. K. Mishra, Trop. Anim. Health Prod. 1990, 22, 63–65, https://doi.org/10.1007/BF02243504.
- [27] S. Salunke-Gawali, E. Pereira, U. A. Dar, S. Bhand, J. Mol. Struct. 2017, 1148, 435–458, https://doi.org/10.1016/j.molstruc.2017.06.130.
- [28] C. Majdi, V. Duvauchelle, P. Meffre, Z. Benfodda, Biomed. Pharmacother. 2023, 162, 114690, https://doi.org/10.1016/j.biopha.2023.114690.
- [29] R. A. Grandis, P. W. D. S. D. Santos, K. M. D. Oliveira, A. R. T. Machado, A. F. Aissa, A. A. Batista, L. M. G. Antunes, F. R. Pavan, *Bioorg. Chem.* 2019, 85, 455–468, https://doi.org/10.1016/j.bioorg.2019.02.010.
- [30] K. M. Oliveira, J. Honorato, F. C. Demidoff, M. S. Schultz, C. D. Netto, M. R. Cominetti, R. S. Correa, A. A. Batista, *J. Inorg. Biochem.* 2021, 214, 111289, https://doi.org/10.1016/j.jinorgbio.2020.111289.
- [31] R. A. Grandis, A. R. Costa, C. A. F. Moraes, N. Z. Sampaio, I. H. Cerqueira, W. G. Marques, A. P. M. Guedes, J. H. De Araujo-Neto, F. R. Pavan, F. C. Demidoff, C. D. Netto, A. A. Batista, F. A. Resende, J. Inorg. Biochem. 2022, 237, 112005, https://doi.org/10.1016/j.jinorgbio.2022.112005.
- [32] A. S. Souza, D. S. Dias, R. C. B. Ribeiro, D. C. S. Costa, M. G. Moraes, D. R. Pinho, M. E. G. Masset, L. M. Marins, S. P. Valle, C. J. C. Carvalho, G. S. G. Carvalho, A. L. N. Mello, M. Sola-Penna, M. V. Palmeira-Mello, R. A. Conceição, C. R. Rodrigues, A. M. T. Souza, L. D. S. M. Forezi, P. Zancan, V. F. Ferreira, F. D. C. Silva, Bioorg. Med. Chem. 2024, 102, 117671, https://doi.org/10.1016/j.bmc.2024.117671.
- [33] P. S. M. Pinheiro, L. S. Franco, T. L. Montagnoli, C. A. M. Fraga, Expert Opin. Drug Discov. 2024, 19, 451–470, https://doi.org/10.1080/17460441. 2024.2322990.
- [34] R. Leechaisit, P. Mahalapbutr, P. Boonsri, K. Karnchanapandh, T. Rungrotmongkol, V. Prachayasittikul, S. Prachayasittikul, S. Ruchirawat, V. Prachayasittikul, R. Pingaew, ACS Omega 2023, 8, 32593–32605, https://doi.org/10.1021/acsomega.3c03176.
- [35] F. Demidoff, F. Souza, C. Netto, Synthesis 2017, 49, 5217–5223.
- [36] F. C. Demidoff, E. J. P. Rodrigues Filho, A. L. F. De Souza, C. D. Netto, L. L. De Carvalho, Synthesis 2021, 53, 4097–4109, https://doi.org/10.1055/s-0037-1610781.
- [37] T. Shen, X. N. Wang, H. X. Lou, *Nat. Prod. Rep.* 2009, 26, 916, https://doi. org/10.1039/b905960a.
- [38] E. Giacomini, S. Rupiani, L. Guidotti, M. Recanatini, M. Roberti, Curr. Med. Chem. 2016, 23, 2439–2489, https://doi.org/10.2174/ 0929867323666160517121629.
- [39] N. F. B. Azeredo, F. P. Souza, F. C. Demidoff, C. D. Netto, J. A. L. C. Resende, R. W. A. Franco, P. Colepicolo, A. M. C. Ferreira, C. Fernandes, J. Mol. Struct. 2018, 1152, 11–20, https://doi.org/10.1016/j.molstruc.2017.08.
- [40] C. M. Leite, J. H. Araujo-Neto, A. P. M. Guedes, A. R. Costa, F. C. Demidoff, C. D. Netto, E. E. Castellano, O. R. Nascimento, A. A. Batista, *Inorganics* 2023, 11, 367.
- [41] S. Kozieł, D. Wojtala, M. Szmitka, J. Sawka, U. K. Komarnicka, Front. Chem. Biol. 2024, 3, 1337372.
- [42] B. Meunier, A. Robert, G. Crisponi, V. Nurchi, J. I. Lachowicz, M. Nairz, G. Weiss, A. B. Pai, R. J. Ward, R. R. Crichton, Essential metals in medicine: Therapeutic use and toxicity of metal ions in the clinic, Walter De Gruyter GmbH & Co KG, Berlin 2019.
- [43] M. Lv, M. Chen, R. Zhang, W. Zhang, C. Wang, Y. Zhang, X. Wei, Y. Guan, J. Liu, K. Feng, M. Jing, X. Wang, Y. C. Liu, Q. Mei, W. Han, Z. Jiang, Cell Res. 2020, 30, 966–979, https://doi.org/10.1038/s41422-020-00395-4.
- [44] L. Cai, Y. Wang, Y. Chen, H. Chen, T. Yang, S. Zhang, Z. Guo, X. Wang, Chem. Sci. 2023, 14, 4375–4389, https://doi.org/10.1039/D2SC06036A.
- [45] N. Mone, S. Harihar, S. Salunke-Gawali, S. Satpute, A. Patil, V. Mokashi, M. Jadhav, R. J. Butcher, *Inorg. Chim. Acta* 2023, 546, 121290, https://doi. org/10.1016/j.ica.2022.121290.
- [46] I. Ali, W. A. Wani, K. Saleem, Synth. React. Inorg., Met.-Org., Nano-Met. Chem. 2013, 43, 1162–1170, https://doi.org/10.1080/15533174.2012.756898.
- [47] N. R. Dhumal, A. V. Todkary, S. Y. Rane, S. P. Gejji, Theor. Chem. Acc. 2005, 113, 161–166, https://doi.org/10.1007/s00214-004-0620-1.
- [48] I. Singh, R. T. Ogata, R. E. Moore, C. W. J. Chang, P. J. Scheuer, *Tetrahedron* 1968, 24, 6053–6073, https://doi.org/10.1016/S0040-4020(01)90989-5.
- [49] K. M. Oliveira, L. D. Liany, R. S. Corrêa, V. M. Deflon, M. R. Cominetti, A. A. Batista, J. Inorg. Biochem. 2017, 176, 66–76, https://doi.org/10.1016/j. jinorgbio.2017.08.019.



- [50] F. P. Andrew, P. A. Ajibade, Int. J. Electrochem. Sci. 2021, 16, 150950, https://doi.org/10.20964/2021.01.65.
- [51] G. J. Islam, H. M. Naseem Akhtar, M. A. Mamun, M. Q. Ehsan, J. Saudi Chem. Soc. 2009, 13, 177-183, https://doi.org/10.1016/j.iscs.2009.05.002.
- [52] Z. Mtshali, K. G. Von Eschwege, J. Conradie, Electrochim. Acta 2021, 391, 138965, https://doi.org/10.1016/j.electacta.2021.138965.
- [53] S. Carli, E. Benazzi, L. Casarin, T. Bernardi, V. Bertolasi, R. Argazzi, S. Caramori, C. A. Bignozzi, Phys. Chem. Chem. Phys. 2016, 18, 5949-5956, https://doi.org/10.1039/C5CP05524E.
- [54] Y. Song, G. R. Buettner, Free Radic. Biol. Med. 2010, 49, 919–962, https:// doi.org/10.1016/j.freeradbiomed.2010.05.009.
- M. V. P. Mello, G. Cebrián-Torreión, J. R. Pereira, C. Santos Moreira, C. B. D. S. M. R. Gomes, D. R. Da Rocha, E. M. S. Fagundes, G. B. Ferreira, M. Lanznaster, J. Inorg. Biochem. 2019, 199, 110756, https://doi.org/10.1016/j. iinorabio 2019 110756
- [56] F. Caruso, M. A. Martínez, M. Rossi, A. Goldberg, M. E. Chacón Villalba, P. J. Aymonino, Inorg. Chem. 2009, 48, 3529-3534.
- [57] S. Oramas-Royo, C. Torrejón, I. Cuadrado, R. Hernández-Molina, S. Hortelano, A. Estévez-Braun, B. L. Heras, Bioorg. Med. Chem. 2013, 21, 2471-2477, https://doi.org/10.1016/j.bmc.2013.03.002.
- [58] J. Castro, E. Manrique, M. Bravo, M. Vilanova, A. Benito, X. Fontrodona, M. Rodríguez, I. Romero, J. Inorg. Biochem. 2018, 182, 124-132, https://doi. org/10.1016/j.jinorgbio.2018.01.021.
- C. Icsel, V. T. Yilmaz, Ş. Aydinlik, M. Aygun, Eur. J. Med. Chem. 2020, 202, 112535, https://doi.org/10.1016/j.ejmech.2020.112535.
- [60] R. Farghadani, J. Rajarajeswaran, N. B. Mohd Hashim, M. A. Abdulla, S. Muniandy, RSC Adv. 2017, 7, 24387-24398.
- [61] M. V. Palmeira-Mello, T. Teixeira, M. R. S. De Melo, H. D. Nicolella, J. L. Dutra, M. R. Cominetti, F. V. Rocha, D. C. Tavares, A. A. Batista, J. Inorg. Biochem. 2025, 265, 112819, https://doi.org/10.1016/j.jinorgbio.2024.11 2819.
- [62] X. An, W. Yu, J. Liu, D. Tang, L. Yang, X. Chen, Cell Death Dis. 2024, 15, 556, https://doi.org/10.1038/s41419-024-06939-5.
- [63] S. Sharkawy, A. Hernández-García, H. Kostrhunova, D. Bautista, L. Markova, M. D. Santana, J. Kasparkova, V. Brabec, J. Ruiz, Inorg. Chem. Front. 2025, 12, 1693-1715, https://doi.org/10.1039/D4QI02737J.
- [64] M. S. Camargo, R. A. Grandis, A. C. Galo, F. A. Resende, P. H. S. Marcon, J. Ellena, J. H. Araujo-Neto, A. A. Batista, J. Inorg. Biochem. 2025, 272, 113008, https://doi.org/10.1016/j.jinorgbio.2025.113008.
- [65] L. Andrezálová, Z. Országhová, J. Inorg. Biochem. 2021, 225, 111624, https://doi.org/10.1016/j.jinorgbio.2021.111624.
- [66] B. J. Pages, D. L. Ang, E. P. Wright, J. R. Aldrich-Wright, Dalton Trans. 2015, 44, 3505-3526, https://doi.org/10.1039/C4DT02700K.
- O. M. Ganguly, S. Moulik, Dalton Trans. 2023, 52, 10639-10656, https:// doi.org/10.1039/D3DT00659J.
- [68] B. Nordén, A. Rodger, T. Dafforn, Linear dichroism and circular dichroism: a textbook on polarized-light spectroscopy, Royal Society of Chemistry, Cambridge 2019
- [69] M. Vorlíčková, I. Kejnovská, K. Bednářová, D. Renčiuk, J. Kypr, Chirality 2012, 24, 691-698.

- [70] M. V. Palmeira-Mello, A. B. Caballero, A. Lopez-Espinar, G. P. Guedes, A. Caubet, A. M. T. Souza, M. Lanznaster, P. Gamez, J. Biol. Inorg. Chem. 2021, 26, 727-740, https://doi.org/10.1007/s00775-021-01888-2.
- [71] N. N. P. Silva, M. V. Palmeira-Mello, N. O. Acésio, C. A. F. Moraes, J. Honorato, E. E. Castellano, D. C. Tavares, K. M. Oliveira, A. A. Batista, Dalton Trans. 2025, 54, 605-615, https://doi.org/10.1039/D4DT02575J.
- Y. Z. Cheng, L. L. Lv, L. L. Zhang, Y. Tang, L. P. Zhang, J. Mol. Struct. 2021, 1228, 129745, https://doi.org/10.1016/j.molstruc.2020.129745.
- [73] M. S. Deshpande, A. A. Kumbhar, A. S. Kumbhar, M. Kumbhakar, H. Pal, U. B. Sonawane, R. R. Joshi, *Bioconjugate Chem.* 2009, 20, 447–459, https://doi.org/10.1021/bc800298t.
- [74] C. Qiu-Yun, Z. Dong-Fang, H. Juan, G. Wen-Jie, G. Jing, J. Inorg. Biochem. 2010, 104, 1141-1147, https://doi.org/10.1016/j.jinorgbio.2010.06.012.
- [75] B. A. Iglesias, N. P. Peranzoni, S. I. Faria, L. B. Trentin, A. P. Schuch, O. A. Chaves, R. R. Bertoloni, S. Nikolaou, K. T. De Oliveira, Molecules 2023, 28,
- [76] J. B. Chaires, Arch. Biochem. Biophys. 2006, 453, 26-31, https://doi.org/10. 1016/j.abb.2006.03.027.
- G. M. Sheldrick, Acta Crystallogr. Sect. A Found. Crystallogr. 2015, 71, 3-8, https://doi.org/10.1107/S2053273314026370.
- [78] H. Puschmann, O. Dolomanov, Acta Crystallogr. Sect. A Found. Adv. 2019, 75, e766-e766, https://doi.org/10.1107/S2053273319087904.
- [79] C. F. Macrae, I. Sovago, S. J. Cottrell, P. T. A. Galek, P. McCabe, E. Pidcock, M. Platings, G. P. Shields, J. S. Stevens, M. Towler, P. A. Wood, Acta Crystallogr. Sect. D Appl. Crystallogr. 2020, 53, 226-235, https://doi.org/10.1107/ S1600576719014092.
- [80] M. Frisch, G. Trucks, H. Schlegel, G. Scuseria, M. Robb, J. Cheeseman, G. Scalmani, V. Barone, G. Petersson, H. Nakatsuii, "Gaussian 16 Revision C. 01, 2016"Gaussian Inc., Wallingford CT 2016, 1, 572.
- [81] C. Lee, W. Yang, R. G. Parr, Phys. Rev. B 1988, 37, 785-789, https://doi.org/ 10.1103/PhysRevB.37.785.
- [82] A. D. Becke, J. Chem. Phys. 1993, 98, 5648-5652, https://doi.org/10.1063/1. 464913.
- [83] P. J. Stephens, F. J. Devlin, C. F. Chabalowski, M. J. Frisch, J. Phys. Chem. 1994, 98, 11623-11627, https://doi.org/10.1021/j100096a001.
- [84] P. C. Hariharan, J. A. Pople, Theoretica Chimica Acta 1973, 28, 213-222, https://doi.org/10.1007/BF00533485.
- G. Scalmani, M. J. Frisch, J. Chem. Phys. 2010, 132, 114110, https://doi.org/ 10.1063/1.3359469
- T. Mosmann, J. Immunol. Methods 1983, 65, 55-63, https://doi.org/10. 1016/0022-1759(83)90303-4.
- [87] M. V. Palmeira-Mello, T. Teixeira, A. R. Costa, A. M. Machado, R. A. Grandis, L. P. Oliveira, C. A. F. Moraes, J. H. Araujo-Neto, V. M. Deflon, A. D. Andricopulo, J. Ellena, H. S. Selistre-de-Araújo, F. V. Rocha, A. A. Batista, Inorg. Chem. Front. 2025, 12, 4812-4827, https://doi.org/10.1039/ D50I00546A.

Manuscript received: July 24, 2025